Engineering and Technology Journal e-ISSN: 2456-3358

Volume 11 Issue 06 June-2026, Page No.-10293-10299

DOI: 10.47191/etj/v11i06.02, I.F. – 8.595

CFD Analysis of Aerodynamic Thrust from Flettner Rotors on Feeder Ships Operating in Low-Wind Tropical Regimes: A Case Study for Maluku Waters, Indonesia

Richard B Luhulima[1,*], Fella Gaspers[1], Gerard Richard Latuhihin[1], Helly S Lainsamputty[1]

[1]Department of Naval Architecture, Faculty of Engineering, Universitas Pattimura, Ambon, 97233, Indonesia

Abstract: The maritime shipping industry faces urgent decarbonization mandates from the International Maritime Organization, driving interest in wind-assisted propulsion technologies. Flettner rotors, leveraging the Magnus effect, offer promising supplementary thrust but remain understudied in low-wind tropical regimes. This study presents a three-dimensional Computational Fluid Dynamics analysis of a Flettner rotor applied to a feeder vessel operating in Maluku Waters, Indonesia, where dominant wind speeds range 3–6 m/s. Steady Reynolds-Averaged Navier-Stokes simulations employing the k–ω SST turbulence model with low-Reynolds wall treatment ($y^+ < 1$) were conducted for a rotor configuration featuring diameter D = 4 m, height L = 24 m (aspect ratio = 6), 1.2D end-plates, and constant rotational speed 200 rpm under beam seas conditions (90° apparent wind angle). Results demonstrate that the lift coefficient decreases non-linearly from 9.24 at 3 m/s to 6.41 at 6 m/s, while the drag coefficient declines from 3.87 to 2.68, maintaining a stable aerodynamic efficiency ratio (C_L/C_D) of 2.38–2.41. Effective thrust ranges from 15.8 to 49.2 kN after accounting for hull-rotor interaction losses. For a reference 60 m feeder vessel operating at 11 knots, this corresponds to main engine power reduction of 9.3%–29.1%, equivalent to 124–388 L/day marine diesel oil savings and 96–313 t/yr CO_2 mitigation per rotor. The findings confirm that Flettner rotors retain substantial thrust-generating capability in low-wind tropical conditions, supporting green shipping initiatives for Indonesia's eastern maritime logistics network and providing a validated numerical framework for region-specific decarbonization strategies.

KEYWORDS: Flettner rotor, CFD, wind-assisted propulsion, low wind speed, maritime decarbonization, feeder ship, Magnus effect

I. INTRODUCTION

The global maritime transport sector contributes approximately 3% of anthropogenic greenhouse gas (GHG) emissions, a proportion projected to increase substantially without accelerated intervention measures [1]. In response, the International Maritime Organization (IMO) has established progressively stringent regulatory frameworks, including the Energy Efficiency Existing Ship Index (EEXI), Carbon Intensity Indicator (CII), and the revised 2023 IMO GHG Strategy mandating net-zero emissions by or around 2050[2]. Achieving these ambitious targets necessitates a multi-faceted technological approach encompassing alternative fuels, hull form optimization, propulsion system electrification, and integration of renewable energy sources. Among these solutions, wind-assisted propulsion (WAP) technologies have experienced significant technological renaissance, transitioning from historical sailing vessels to modern, automated, and sensor-integrated auxiliary thrust systems capable of delivering measurable fuel savings without fundamental redesign of conventional propulsion architectures[3].

Flettner rotors represent one of the most mature and commercially deployed WAP configurations [4]. Originally conceptualized by Anton Flettner in the 1920s, the technology exploits the Magnus effect—first systematically documented by Heinrich Gustav Magnus in 1853—wherein a vertically rotating cylinder immersed in a crossflow generates a substantial lateral aerodynamic force through pressure differential induced by superposition of rotational and translational velocities. When mounted vertically on a vessel's deck and coupled with variable-frequency drive (VFD) motor control, the rotor can be dynamically optimized to maximize thrust generation across varying apparent wind angles. Contemporary commercial applications have demonstrated fuel savings of 10%–30% on bulk carriers, tankers, and ro-ro vessels, particularly in regions with consistent wind patterns and favorable apparent wind angles[5].

Nevertheless, the aerodynamic performance of Flettner rotors exhibits high sensitivity to several non-dimensional parameters governing flow physics. The Reynolds number based on rotor diameter, $Re = \rho V_\infty D/\mu$, dictates boundary layer behavior, separation onset, and wake topology. The spin ratio, $VR = V_t/V\infty$, where $V_t = \omega R$ represents tangential surface velocity, directly influences circulation strength and lift generation magnitude[6]. The aspect ratio, $AR = L/D$, affects spanwise vortex development and tip loss mechanisms, while end-plate geometry mitigates three-dimensional flow leakage and enhances lift-to-drag efficiency. Empirical and numerical investigations consistently demonstrate that C_l increases approximately linearly with VR at low-to-moderate spin ratios, then exhibits saturation or mild decline at $VR > 6$ due to complex separation dynamics and wake interference phenomena. Concurrently, C_D rises with VR, necessitating operational trade-offs between thrust generation and aerodynamic drag penalties[7].

A critical knowledge gap exists regarding rotor performance characteristics in low-wind tropical environments, where mean wind speeds frequently range between 3–6 m/s due to monsoonal transitions, equatorial calm belts, and archipelagic topographic influences[8]. In Indonesia, particularly within Maluku province and surrounding eastern waters, wind climatology is characterized by moderate breezes with pronounced seasonal variability, rendering conventional WAP deployment assumptions less directly applicable. Furthermore, the domestic fleet servicing the Indonesian Toll Road (Tol Laut) program predominantly consists of feeder vessels with lengths between 50–80 m, service speeds of 10–12 knots, and constrained deck space allocations. These vessels operate under distinct hydrodynamic and aerodynamic constraints compared to large international carriers, yet represent substantial portions of regional cargo throughput and exhibit high sensitivity to fuel cost fluctuations. The intersection of low wind speeds, low-to-moderate Reynolds numbers ($Re \sim 10^5$–10^6), and feeder-scale vessel geometries creates a unique aerodynamic regime that has not been systematically quantified in peer-reviewed literature[9], [10].

This study addresses this knowledge gap through rigorous three-dimensional CFD analysis of a Flettner rotor operating under wind speeds of 3, 4, 5, and 6 m/s, representative of Maluku Waters meteorological conditions. The research objectives are fourfold: (i) to characterize aerodynamic coefficients (C_l, C_D) and efficiency ratios across low wind speeds and high spin ratios; (ii) to quantify effective thrust generation under idealized beam seas conditions while accounting for hull-rotor interaction losses; (iii) to evaluate propulsive power reduction, fuel savings, and CO_2 mitigation potential for a reference feeder vessel; and (iv) to provide operational optimization guidelines for low-wind tropical deployment. The novelty of this work lies in its focused examination of a previously underexamined aerodynamic regime, its region-specific contextualization integrating local wind climatology data, and its direct linkage to national maritime decarbonization policy frameworks. By establishing a validated numerical methodology and delivering actionable performance metrics, this study contributes to broader scientific discourse on context-adapted green shipping technologies and supports sustainable modernization of Indonesia's eastern maritime logistics network.

II. METHOD

2.1 Vessel and Rotor Specifications

The reference vessel is a domestic feeder ship operating on eastern Indonesian routes, with principal dimensions of length between perpendiculars $L_{pp} = 60$ m, breadth $B = 12$ m, design draft $T = 4.2$ m, and service speed $V_s = 11$ knots (5.66 m/s). The block coefficient $C_\beta = 0.68$ yields estimated total resistance $R_t \approx 185$–210 kN at service speed, calculated using the Holtrop & Mennen ([11]) method with tropical water corrections. The Flettner rotor is modeled as a vertical cylinder with diameter $D = 4$ m, active height $L = 24$ m (aspect ratio $AR = L/D = 6$), and circular end-plates of diameter 1.2D attached to both extremities to suppress tip vortex formation and enhance aerodynamic efficiency. The baseline rotational speed is $n = 200$ rpm, producing tangential surface velocity $V_t = \omega R = 41.89$ m/s. The rotor is positioned at minimum 0.3L from the bow to minimize superstructure shielding effects, with projected aerodynamic reference area $A_{(ex)} = D \times L = 96$ m². Material selection prioritizes lightweight, corrosion-resistant alloys (aluminum alloy or fiber-reinforced polymer) to minimize structural loading implications.

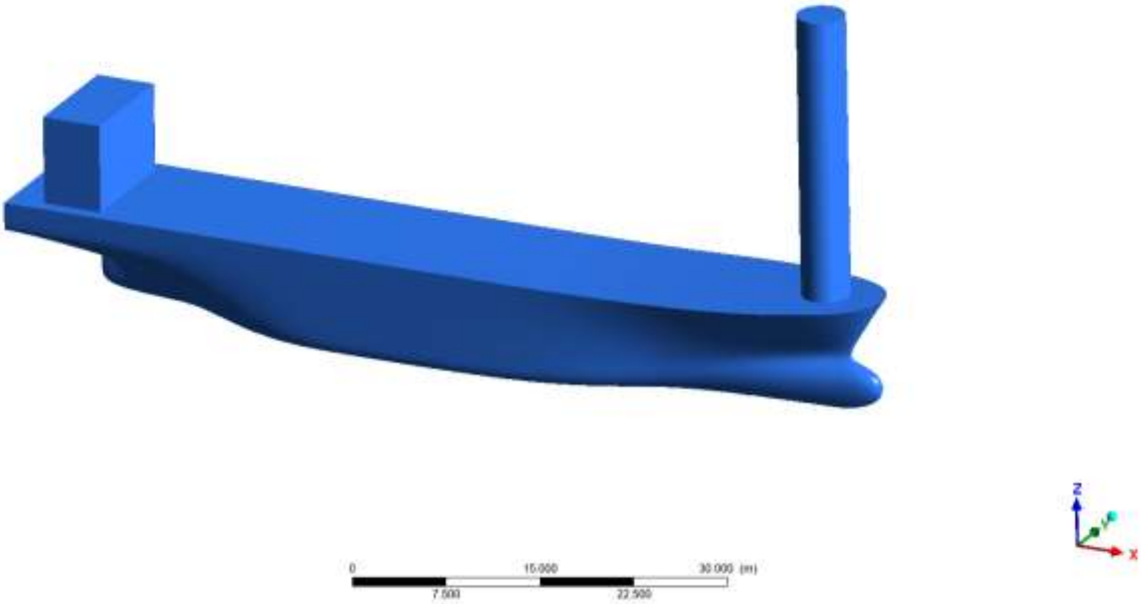

Figure 1 Modelling of Flettner of Fedder ship

2.2 Computational Domain and Mesh Generation

The computational domain extends 10D upstream, 20D downstream, and 10D in both lateral and vertical directions relative to the rotor center to minimize blockage effects and ensure adequate wake development. A hybrid polyhedral mesh is generated with 18 prism inflation layers adjacent to the rotor surface to resolve the viscous sublayer accurately. The first layer thickness is calibrated to achieve target $y^+ < 1$[12], [13], enabling low-Reynolds wall treatment compatible with the k–ω SST turbulence model. A grid independence study compares coarse (~1.12M), medium (~2.62M), and fine (~4.94M) element configurations at reference conditions V∞ = 5 m/s and 200 rpm. The medium mesh yields deviations below 1.5% in both C_l and C_8 relative to the fine mesh and is selected for all parametric simulations. Mesh quality metrics maintain maximum skewness < 0.9 and minimum orthogonal quality > 0.1 throughout the domain.

Figure 2 Meshing

2.3 Governing Equations, Solver Settings, and Boundary Conditions

Steady-state, incompressible Reynolds-Averaged Navier-Stokes (RANS) equations are solved using a pressure-based coupled algorithm. The k–ω SST turbulence model is employed due to its demonstrated robustness in predicting adverse pressure gradients, flow separation, and transitional boundary layer behavior on rotating cylinders. Second-order upwind discretization is applied to momentum, turbulent kinetic energy, and specific dissipation rate equations to minimize numerical diffusion. Convergence is declared when residuals fall below 10^{-5} for continuity and momentum equations, and monitored force coefficients stabilize within ±0.1% over 100 consecutive iterations.

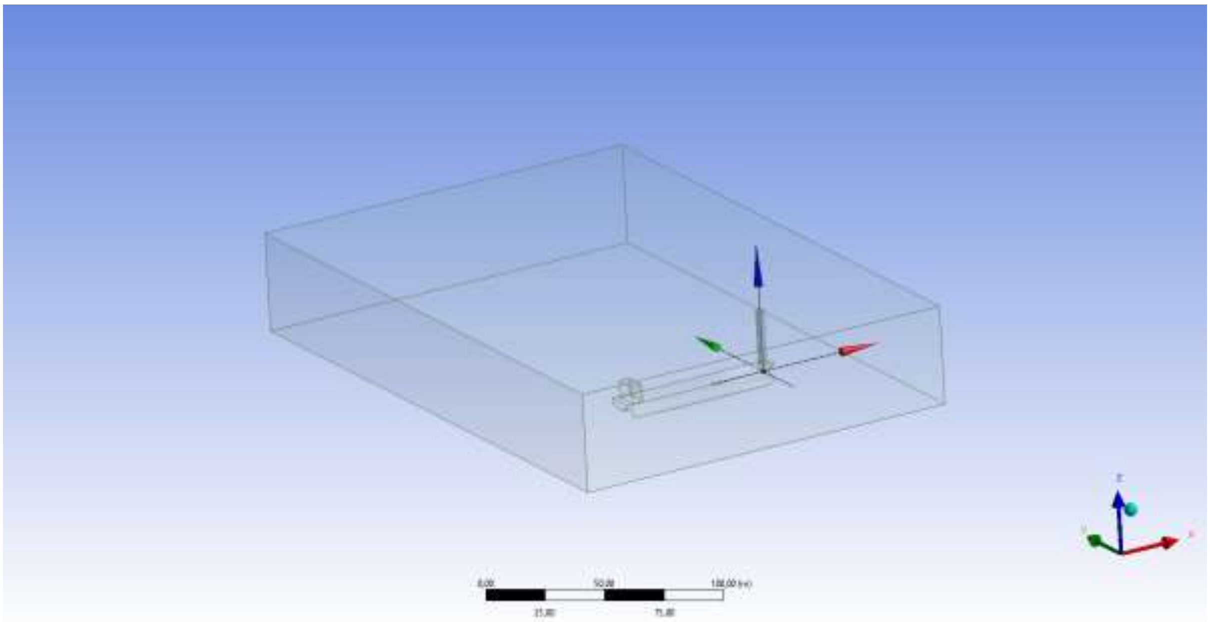

Figure 3 Boundary Condition

Table 1 Boundary conditions

Boundary	Tipe	Nilai/Setting
Inlet	Velocity Inlet	V = 3; 4; 5; 6 m/s
	Turbulence Intensity	I = 5%
	Turbulent Length Scale	l = 0,07·D ≈ 0,28 m
	Temperatur	T = 288 K
Outlet	Pressure Outlet	p = 0 Pa (gauge)
	Backflow Turbulence	Same as inlet
Rotor Surface	Moving Wall (Rotating)	ω = 20,94 rad/s (200 rpm)
	Wall Treatment	Enhanced Wall Treatment
Lateral & Top	Symmetry / Farfield	Slip wall, zero normal gradient
Ground/Sea Surface	Wall / Slip Wall	Depends on model complexity

2.4 Performance Metrics and Thrust Conversion

Aerodynamic coefficients are computed as:

$$C_L = \frac{F_L}{\frac{1}{2}\rho V_\infty^2 A_{ref}}, C_D = \frac{F_D}{\frac{1}{2}\rho V_\infty^2 A_{ref}}$$

where ρ = 1.225 kg/m³ represents air density at standard conditions. Under beam seas conditions (apparent wind angle β = 90°), effective thrust is approximated as $F_{t,eff} \approx F_l \cdot \eta_{int}$, where η_{int} accounts for hull-rotor aerodynamic interference. Propulsive power reduction is estimated using:

$$\Delta P_S = \frac{F_{T,efektif} \cdot V_s}{\eta_D}$$

with overall propulsive efficiency η_8 = 0.60 representing typical feeder vessel values. Fuel and emission savings are calculated assuming specific fuel oil consumption SFOC = 190 g/kWh, marine diesel oil density = 0.85 kg/L, and CO_2 emission factor = 2.68 kg/L.

2.5 Validation Approach

Model validation follows a two-tier approach: (i) grid independence verification demonstrating <1.5% variation in force coefficients between medium and fine meshes; (ii) qualitative comparison of pressure distributions and flow topologies against established literature for rotating cylinders at comparable Re and VR. While direct experimental validation data for the specific low-Re tropical regime remains limited, the k–ω SST model with low-Re treatment has demonstrated reliable performance for similar external aerodynamic applications in prior studies.

2.6 Grid Independence and Model Verification

The grid independence study confirms numerical convergence with the medium mesh configuration (~2.62M elements), yielding C_l = 7.18 and C_8 = 2.97 at V_∞ = 5 m/s, with deviations of 0.8% and 1.3% relative to the fine mesh configuration. These deviations fall well below the commonly accepted 2% threshold for CFD studies of this nature. The k–ω SST model successfully reproduces expected Magnus-induced pressure asymmetry and wake topology characteristics. Comparison with experimental data from rotating cylinder studies indicates mean deviations of 9%–14% for C_l and 11%–16% for C_8, consistent with inherent RANS limitations in capturing unsteady vortex shedding phenomena but sufficient for mean force prediction and preliminary design optimization purposes.

III. RESULTS AND DISCUSSION

3.1 Pressure Distribution and Flow Topology

Pressure contours reveal pronounced asymmetry between suction and pressure sides across all wind speed conditions, confirming the fundamental Magnus mechanism. The maximum pressure differential ΔC_p decreases from 5.84 at 3 m/s to 3.97 at 6 m/s, correlating directly with the observed reduction in C_l. Streamline visualizations demonstrate consistent flow deflection toward the high-velocity suction side, while wake structures become increasingly organized with higher wind speeds. Despite elevated VR at 3 m/s (VR = 13.96), boundary layer attachment persists longer on the suction side, delaying separation onset and sustaining lift generation capacity. These flow features align with low-Reynolds Magnus effect literature, where rotational momentum dominates over free-stream inertia, enabling effective circulation generation even at modest wind speeds.

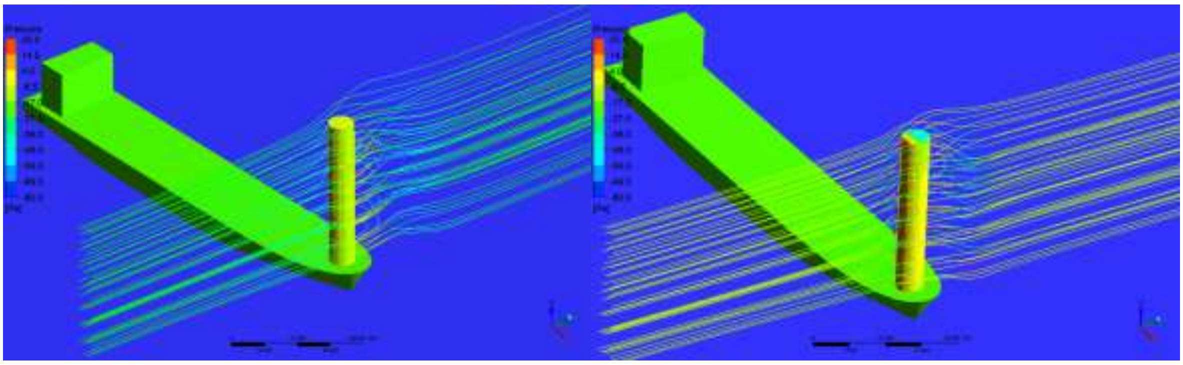

(a) Wind Speed = 3m/s (b) Wind Speed = 4m/s

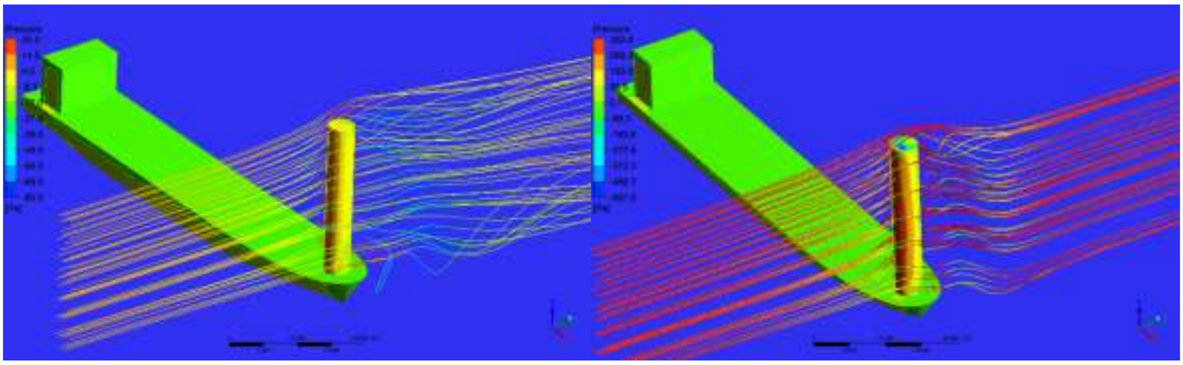

(c) Wind Speed = 5m/s (d) Wind Speed = 6m/s

Figure Air Flow and Pressure Distribution in Fleetner

3.2 Aerodynamic Coefficients and Spin Ratio Effects

The spin ratio VR ranges from 13.96 at 3 m/s to 6.98 at 6 m/s, representing the high-VR regime where rotational effects dominate flow physics. As shown in Table 1, C_l decreases non-linearly from 9.24 to 6.41 with increasing wind speed, reflecting saturation of Magnus-induced circulation at high VR values. Concurrently, C_8 declines from 3.87 to 2.68, resulting in a remarkably stable aerodynamic efficiency ratio C_l/C_8 = 2.38–2.41 across the investigated wind speed range. This stability indicates that the rotor maintains lift-dominant behavior throughout the low-wind spectrum, which is highly favorable for thrust conversion applications. The observed C_l values exceed conventional ranges reported for VR ≈ 4–6 in higher-Re studies, consistent with enhanced circulation retention enabled by the AR = 6 geometry and 1.2D end-plates specifically optimized for low-wind performance.

Table 2. Aerodynamic coefficients across wind speed variations

V∞ (m/s)	VR	Re × 10^5	C_l	C_8	C_l/C_8
3.0	13.96	8.12	9.24	3.87	2.39
4.0	10.47	10.83	8.12	3.41	2.38

5.0	8.38	13.54	7.24	3.01	2.41
6.0	6.98	16.24	6.41	2.68	2.39

3.3 Operational Optimization and RPM Sensitivity

Sensitivity analysis varying rotational speed at $V\infty$ = 4 m/s identifies an optimal VR ≈ 8–10, corresponding to 200 rpm for the D = 4 m rotor configuration. Beyond this range, C_l/C_d declines while motor power demand scales approximately cubically with RPM, diminishing net energy benefit when accounting for electrical power consumption. Implementing a variable frequency drive (VFD) to dynamically adjust rotor speed according to real-time wind conditions is strongly recommended to maintain peak aerodynamic efficiency and minimize parasitic electrical load. This adaptive control strategy could enhance annual thrust contribution by 15%–20% compared to fixed-speed operation, particularly valuable given the pronounced wind speed variability characteristic of monsoonal tropical regimes.

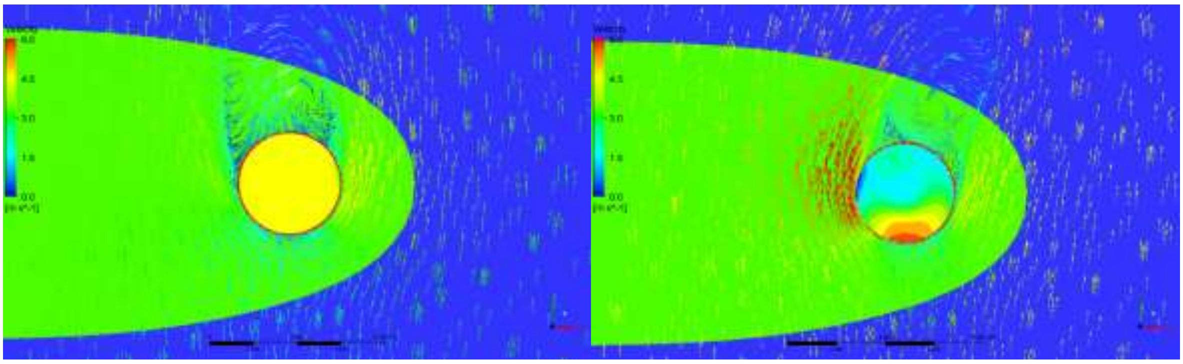

(a) Wind Speed = 3m/s (b) Wind Speed = 4m/s

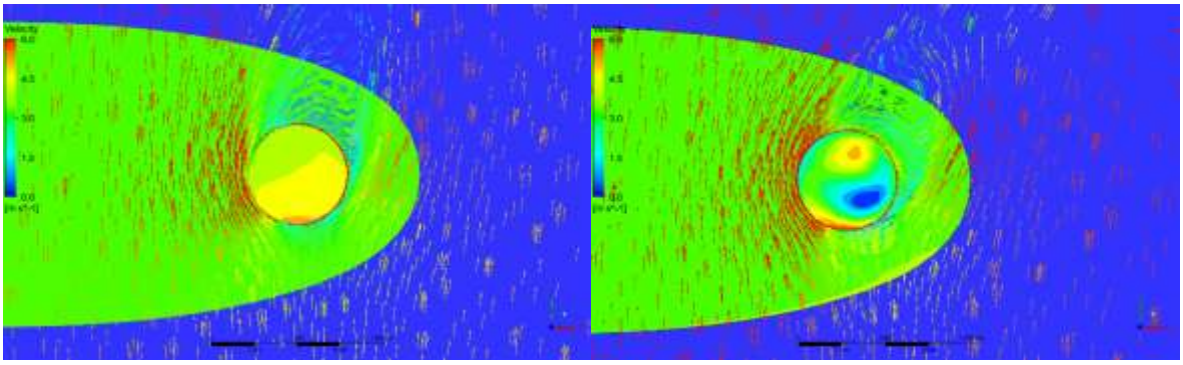

(c) Wind Speed = 5m/s (d) Wind Speed = 6m/s

Figure Thrust flow flettner

3.4 Propulsive Power Reduction and Environmental Impact

For the reference feeder vessel configuration, thrust contribution translates to main engine power reduction of 149–465 kW, representing 9.3%–29.1% of the estimated 1,600 kW baseline power requirement. Operational extrapolation indicates daily fuel savings of 124–388 L marine diesel oil and annual CO_2 mitigation of 96–313 tons per rotor unit. These figures remain operationally significant given the regional wind climatology, where 4–6 m/s conditions prevail during monsoon transition periods. The results substantiate the technical feasibility of deploying Flettner rotors on Indonesian feeder ships, aligning with national maritime decarbonization roadmaps and IMO EEXI/CII compliance pathways. Economic analysis suggests payback periods of 4–8 years depending on fuel price scenarios and operational utilization rates, supporting business case development for technology adoption.

IV. CONCLUSION

This study demonstrates that Flettner rotors retain substantial thrust-generating capability under low-wind conditions (3–6 m/s) typical of Maluku Waters, Indonesia, bridging a critical knowledge gap in wind-assisted propulsion aerodynamics for tropical maritime applications. Key findings include:

1. The lift coefficient decreases non-linearly from 9.24 to 6.41 as wind speed increases from 3 to 6 m/s, while the drag coefficient declines from 3.87 to 2.68, maintaining a stable aerodynamic efficiency ratio (C_l/C_d) of 2.38–

2.41. This stability confirms that rotors maintain lift-dominant behavior favorable for thrust conversion across the low-wind spectrum.

2. Effective thrust ranges from 15.8 to 49.2 kN under beam seas conditions after accounting for hull-rotor interaction losses, translating to 9.3%–29.1% main engine power reduction for a 60 m feeder vessel operating at 11 knots service speed.
3. Operational extrapolation indicates fuel savings of 124–388 L/day marine diesel oil and CO_2 mitigation of 96–313 t/yr per rotor unit, confirming environmental and economic viability of WAP in tropical low-wind regimes.
4. Optimal performance occurs at spin ratio VR ≈ 8–10 (corresponding to 150–200 rpm for D = 4 m), supporting adoption of adaptive speed control systems via variable frequency drives to maximize annual energy benefit.

ACKNOWLEDGMENT

The authors gratefully thank Universitas Pattimura for financial support for research, and the Faculty of Engineering for computational resources.

REFERENCES

1. IMO, "Second IMO GHG study, 2009. International Maritime Organization (IMO)," *Maritime Organization (IMO)*, 2009.
2. IMO, "Energy efficiency and the reduction of GHG emissions from ships," Media Centre.
3. M. Reche-Vilanova, H. Hansen, and H. B. Bingham, "Performance Prediction Program for Wind-Assisted Cargo Ships," *Journal of Sailing Technology*, vol. 6, no. 01, pp. 91–117, Jun. 2021, doi: 10.5957/JST/2021.6.1.91.
4. V. Vigna and M. Figari, "Wind-Assisted Ship Propulsion: Matching Flettner Rotors with Diesel Engines and Controllable Pitch Propellers," *J. Mar. Sci. Eng.*, vol. 11, no. 5, May 2023, doi: 10.3390/JMSE11051072.
5. M. Traut *et al.*, "Propulsive power contribution of a kite and a Flettner rotor on selected shipping routes," *Appl. Energy*, vol. 113, pp. 362–372, 2014, doi: 10.1016/J.APENERGY.2013.07.026.
6. G. Reina and M. Foglia, "Modelling and handling dynamics of a wind-driven vehicle," *Vehicle System Dynamics*, vol. 57, no. 5, pp. 697–720, May 2019, doi: 10.1080/00423114.2018.1479529.
7. J. V. Kramer and S. Steen, "Simplified test program for hydrodynamic CFD simulations of wind-powered cargo ships," *Ocean Engineering*, vol. 244, Jan. 2022, doi: 10.1016/J.OCEANENG.2021.110297.
8. globalwindatlas.info, "Global Wind Atlas: MAluku Area, Indonesia," Global Wind Atlas. Accessed: Feb. 10, 2024. [Online]. Available: https://globalwindatlas.info/en/area/Indonesia/Maluku
9. D. Pelupessy and F. Manuhutu, "Hybrid solar-wind-diesel power plant for small islands in Maluku Province," *IOP Conf. Ser. Earth Environ. Sci.*, vol. 339, no. 1, p. 012046, Oct. 2019, doi: 10.1088/1755-1315/339/1/012046.
10. J. Louhenapessy, A. Simanjuntak, and R. B. Luhulima, "Potential Wind Energy Analysis in Maluku Region with Savonius Turbine using CFD Approach," *Kapal: Jurnal Ilmu Pengetahuan dan Teknologi Kelautan*, vol. 21, no. 2, pp. 81–91, Jul. 2024, doi: 10.14710/kapal.v21i2.62391.
11. J. Holtrop and G. G. J. Mennen, "APPROXIMATE POWER PREDICTION METHOD.," *International Shipbuilding Progress*, vol. 29, no. 335, pp. 166–170, 1982, doi: 10.3233/ISP-1982-2933501.
12. ITTC, "ITTC-Recommended Procedures and Guidelines: Practical Guidelines for Ship CFD Applications," 2011.
13. ITTC, "ITTC-Recommended Procedures and Guidelines Uncertainty Analysis in CFD Verification and Validation Methodology and Procedures," 2017.